Spacer-induced forward osmosis membrane integrity loss during gypsum scaling

Spacer-induced Forward Osmosis Membrane Integrity Loss during Gypsum Scaling

Desalination

Revised: April 2016

Ming Xie [1*], Chuyang Y. Tang [2] and Stephen R. Gray [1]

[1] Institute for Sustainability and Innovation, College of Engineering and Science, Victoria University, PO Box 14428, Melbourne, Victoria 8001, Australia

[2] Department of Civil Engineering, The University of Hong Kong, Hong Kong

* Corresponding author: M.X., email: ming.xie@vu.edu.au; phone: +61 3 9919 8174

ABSTRACT

We demonstrated forward osmosis (FO) membrane integrity loss during gypsum scaling with the presence of membrane spacer. The gypsum scalant had preferential accumulation adjacent to membrane spacer where the needle-shape gypsum potentially compromised polyamide thin-film composite FO membrane integrity. However, the loss of FO membrane integrity cannot be sensitively detected by *in situ* measurements of membrane water and salt (NaCl) permeability coefficients. We, for the first time, employed membrane integrity challenge tests to reveal the impaired FO membrane integrity by fluorescent Rhodamine WT tracer and amine-modified latex nanoparticles, respectively. Challenge tests using Rhodamine WT tracer showed that membrane log removal value decreased to 3.5 after three scaling-cleaning cycles, which corresponded to a pinhole size of 0.06 μm^2 on the FO membrane surface. This result was further corroborated by challenge tests using latex nanoparticle where the particle size distribution in the permeate became wider and the average particle size increased over the three scaling-cleaning cycles. Both challenge tests were sensitive enough to identify impaired FO membrane integrity. Results reported here have significant implications for achieving better membrane spacer and module design, as well as demanding periodical monitoring of FO membrane integrity in water reuse.

Key words: Forward osmosis; gypsum scaling; membrane integrity; fluorescent Rhodamine WT tracer; amine-modified latex nanoparticle

1. Introduction

Membrane technologies respond to the global challenge for adequate and safe water [1, 2]. Forward osmosis (FO), an emerging osmosis-driven membrane process, has the potential to advance seawater desalination and wastewater reuse [3]. Because of the low fouling propensity and high fouling reversibility with simple membrane flushing, FO has potential applications in treatment of a variety of high fouling potential source waters [4-7], including desalination of high salinity brines from shale gas produced water [8-11], municipal wastewater reclamation [12-16], and valuable resource recovery [17-19].

These challenging waste streams with complex foulants stress membrane mechanical properties and subsequent membrane performance. For instance, recent studies reported minor changes in FO membrane properties and performance after exposure to oil and gas wastewaters [20]. More importantly, damage to FO membrane active layer was visualized after gypsum scaling with the presence of membrane spacers [21]. These prior findings warrant a close examination of FO membrane integrity during processing of wastewaters with high fouling propensity.

Varying techniques were proposed to examine reverse osmosis (RO) membrane integrity, such as fluorescent spectroscopy [22-24], Rutherford backscattering spectrometry [25, 26], and flow cytometry [27]. For instance, fluorescence signatures, such as peak C as $\lambda_{Ex/Em}$= 3000/400 nm, were proposed to monitor RO membrane integrity due to relatively low noise and variability of these fluorescent organic molecules [22]. For biological particles, such as virus, flow cytometry demonstrated good sensitivity and reproducibility for quantifying virus reduction rate along the treatment processes, which provide direct evidence for RO membrane integrity monitoring [27].

These techniques aim to ensure that RO membrane achieves high log removal value (LRV) for virus removal so as to address public health protection concerns, as well as regulatory requirements. However, to date, there is no existing study that examines membrane integrity of FO process, particularly in treatment of high fouling wastewaters. Such fundamental understanding can lead to the development of monitoring techniques for FO membrane integrity, which will significantly increase the efficiency and robustness of FO process.

In this study, we demonstrate that FO membrane integrity was compromised during gypsum scaling. Membrane gypsum scaling was visualized by a real-time observation system. Membrane integrity of three scaling-cleaning cycles was examined using challenge tests comprising sensitive fluorescent Rhodamine WT tracer and amine-modified latex nanoparticles.

2. Materials and methods

2.1 Real-time FO observation system

A transparent, acrylic FO membrane cell coupled with microscopic observation enabled real-time observation of gypsum scaling (Figure S1, Supplementary Data). Specifically, a membrane coupon with an effective area of 20.2 cm^2 was placed in a transparent FO membrane cell. A crossflow rate of 1 L/min (corresponding to crossflow velocity of 9 cm/s) was maintained for both the feed and draw solutions using micro gear pumps. The FO water flux was determined by measuring the weight changes of the feed solution at specific time intervals with a precision balance connected to a computer and a data logging system.

Real-time membrane surface images of 2048 × 1536 pixels resolution were recorded using a high resolution digital camera and an optical microscope (20× magnification). To minimize the interference from air bubbles, the feed and draw solutions were degassed prior to circulation in the FO setup. Through the combination of optical magnification along with a unique combination of bright and low angle dark field illumination, provided by ultra-bright fiber optic illuminator, digital image capture and analysis, occurrence and subtle changes of gypsum crystal could be effectively monitored.

2.2 Membrane and spacer

A polyamide thin-film composite (TFC) forward osmosis (FO) membrane was employed in this study. The TFC membrane was made of a thin selective polyamide active layer on top of a porous polysulfone support layer [28].

Spacers are essential to an FO membrane module to maintain flow channel and provide hydrodynamic conditions. Diamond-patterned, polypropylene spacers (65 mil (1.651 mm) spacer, GE Osmonics), which were also the current standard RO membrane spacer, were placed in both the feed and draw channels during the experiments.

2.3 Experimental protocol for gypsum scaling and cleaning

A total of three gypsum scaling-cleaning cycles were conducted. The protocol for gypsum scaling experiments comprised the following steps. First, a new membrane coupon, with the active layer facing the feed solution, was placed in the membrane cell before each experiment and stabilized to obtain a constant flux. The membrane in the FO mode (i.e., membrane active layer faces feed solution) was stabilized with deionized water feed and 2 M NaCl draw. Next, the gypsum scaling experiment was performed for about 24 h to obtain approximately 1400 mL cumulative permeate volume at the conclusion of each experiment. The gypsum scaling solution was comprised of 35 mM $CaCl_2$, 20mM Na_2SO_4, and 19 mM NaCl, with a gypsum ($CaSO_4 \cdot 2H_2O$) saturation index (SI) of 1.3. Other experimental conditions were: crossflow velocity of 9 cm/s, ambient pH (pH 6.8), and temperature of 25.0 ± 0.1°C. Water flux was continuously monitored throughout the fouling experiments by a data logger. A baseline experiment (i.e., feed without $CaCl_2$ and Na_2SO_4) was also carried out to correct the flux decline due to the continuous concentration of the feed solution and dilution of the draw solution, as described in our previous publication [7]. The real-time monitoring system captured images of the FO membrane surface every 30 minutes during the scaling experiment to identify the occurrence and development of gypsum crystals on FO membrane surface during scaling experiment.

Membrane cleaning was performed immediately after the FO scaling experiments. Deionized water flushing was carried out in both feed and draw flow channels at 18 cm/s for 30 min. The membrane water flux after cleaning was measured using deionized water feed and 2 M NaCl draw.

Key membrane transport parameters (water permeability coefficients, *A* and salt (NaCl) permeability coefficient, *B*) of pristine membrane and membrane after each cycle were determined according to a method previously described [29]. Briefly, the determination of key membrane transport parameters comprises a single FO experiment divided into four stages, each using a different concentration of draw solution. The experimental water and reverse salt fluxes measured in each stage are fitted to the corresponding FO transport equations by performing a least-squares non-linear regression, using *A*, *B*, and *S* as regression parameters. Four different NaCl draw concentrations (approximately 0.2, 0.4, 0.7, and 1.2 M NaCl) were employed. These parameters were adjusted to fit the experimental data of water and reverse salt fluxes to the corresponding governing equations. This method allowed an *in situ* measurement of membrane characteristics *without* taking the FO membrane out of the membrane cell and transferring into a pressurized RO filtration setup, which could potentially impair membrane integrity.

2.4 FO membrane integrity examination

Apart from measuring key membrane transport parameters, FO membrane integrity at the conclusion of each gypsum scaling-cleaning cycle was examined by challenge tests using two tracers: fluorescent Rhodamine WT (Tuner Designs, CA, USA) and amine-modified polystyrene latex nanoparticle (Sigma-Aldrich, MO, USA), respectively. Details regarding these two tracers were provided in the Supplementary Data (Table S1). Specifically, the challenge tests were conducted in single-pass mode where neither feed nor draw solution were returned to their reservoirs. A pulse of either fluorescent Rhodamine WT solution of 50 mg/L or amine-modified polystyrene latex nanoparticle solution of 20 mg/L was injected into the FO feeding tube for 60 seconds at a crossflow rate of 1 L/min (corresponding to crossflow velocity of 9 cm/s). At the same time, the draw solution at a crossflow rate of 1 L/min (corresponding to crossflow velocity of 9 cm/s) was sampled every 10 seconds for a total of 540 seconds to generate either a time-concentration profile of fluorescent Rhodamine WT or the nanoparticle size distribution in the draw solution. A detailed description of challenge tests is provided in the supplementary materials and methods, Supplementary Data. Concentration of fluorescent Rhodamine WT was quantified by a fluorometer (AquaFluor, Tuner Design, CA, USA) at excitation wavelength of 530 nm and emission wavelength of 555 nm. Nanoparticle size distribution was determined by dynamic light scattering (Zetasizer Nano ZSP, Malvern Instruments, Worcestershire, UK).

The log removal value (LRV) of fluorescent Rhodamine WT was calibrated as a function of pinhole size in order to quantify the degree of FO membrane integrity loss. The FO membrane integrity loss was artificially induced by lightly tapping the membrane samples using a tip of a hypodermic needle (GL Sciences, Tokyo, Japan). Pinholes of various sizes (0.02-0.08 μm^2) were created on the FO membrane sample that was subjected to the aforementioned fluorescent Rhodamine WT challenge test. The LRV value was calculated by:

$$LRV = \log\left(\frac{C_{draw}DF}{C_{feed}}\right) \quad (1)$$

where C_{draw} was the Rhodamine WT trace concentration in the draw; DF was the dilution factor of Rhodamine WT trace by considering the draw solution volume; C_{feed} was the Rhodamine WT trace concentration in the feed. It was assumed that the feed Rhodamine WT trace concentration remained constant during the short period of challenge test.

3. Results and Discussion

3.1 Gypsum scalant accumulates adjacent to spacer filament

Membrane spacer significantly affected membrane performance and gypsum scaling pattern. Membrane spacer not only alleviated gypsum scaling (Figure 1A), but also induced preferential accumulation of gypsum scalant adjacent to spacer filament (Figure 1B). Specifically, membrane spacer abated water flux decline by 22% during gypsum scaling in comparison with FO filtration without membrane spacer. The enhanced membrane performance was attributed to the mitigation of concentration polarization at membrane interface by membrane spacer [30-32].

[Figure 1]

More importantly, real-time microscopic observation demonstrated that gypsum scaling was initiated next to spacer filament, and progressively resulted in severe accumulation of gypsum scalant in the confined region close to spacer filament (Figure 1B, and Video S1, Supplementary Data). In comparison with the gypsum scaling without membrane spacer (Figure S4, Supplementary Data), our real-time microscopic imaging showed that gypsum scalant preferentially accumulated adjacent to the membrane spacers. Such gypsum scaling pattern was mainly driven by the hydrodynamic dead zones created near the filaments, thereby favoring the

crystallization and growth of gypsum scalant. Our results also agreed well with prior studies of particulate scaling in FO process, using latex particle [33] and microalgae [34], which preferentially accumulated at regions next to the fabric filaments in the filtration. These observations were consistent with previous knowledge of RO scaling [35-37], that crystal formation and precipitate deposition occurred preferentially at the spacer induced hydrodynamic dead zones.

SEM micrographs of the gypsum-scaled membrane further verified the preferential accumulation of gypsum scalant adjacent to membrane spacers (Figure 2). More importantly, these images also revealed the indentation and possible pinholes on the membrane active layer after removing membrane spacers (Figures 2B and D). As a result, it raised concerns regarding FO membrane integrity when needle-shaped gypsum crystal morphology was revealed in the confined region adjacent to spacer filament (Figure 2). As a result, it was hypothesized that such gypsum scaling pattern could potentially compromise FO membrane integrity, and further evidence to support this hypothesis is provided in the following sections.

[Figure 2]

3.2 Membrane transport parameters measurements cannot identify membrane integrity loss

Key membrane transport parameters – water permeability coefficient, *A*, and salt (NaCl) permeability coefficient, *B* – were measured *in situ* at the conclusion of each scaling-cleaning cycle using a single FO experimental method [29]. This method minimized potential mechanical damage of the FO membrane by undertaking the characterization *in situ*, rather than transforming into and testing by a pressurized RO membrane cell.

Statistically, negligible differences in membrane *A* and *B* values were observed (Figure 3) between pristine membrane and membranes after three scaling-cleaning cycles (student *t*-test, *P* value>0.05). Largely unchanged membrane water and salt (NaCl) permeabilities also agreed with the high water flux recovery (>97%) after membrane physical flushing (Figure S3, Supporting Information), which benefited from the high fouling reversibility of FO process [6, 38, 39]. However, limited variations in water and salt (NaCl) permeability coefficients were not sufficiently sensitive to reflect the potential loss of membrane integrity. As a result, we employed membrane integrity challenge tests comprising two tracers – fluorescent Rhodamine WT and

amine-modified polystyrene latex nanoparticles – to more closely examine membrane integrity during gypsum scaling.

[Figure 3]

3.3 Fluorescent dye tracer and latex nanoparticle challenge tests reveal membrane integrity loss.

Membrane integrity challenge tests were performed by introducing a pulse of tracer that enabled sensitive detection of breach of membrane integrity. Two tracers were used to examine the loss of membrane integrity. First, fluorescent Rhodamine WT, which has been previously used to monitor RO membrane integrity [40], can be detected at low concentration of 0.04 μg L^{-1} using the current analytical method. The intact FO membrane achieved LRV up to 5.1 using fluorescent Rhodamine WT (Figure 4). Second, the amine-modified latex nanoparticles with average particle size of 50 nm, which is equivalent to the size of virus, did not show severe aggregation during of the challenge test (Figure S3, Supplementary Data), which making it an excellent surrogate for FO membrane integrity for virus removal [25].

3.3.1 Fluorescent Rhodamine WT challenge test

Concentration-time profile of Rhodamine WT demonstrated a progressive increase of Rhodamine WT concentration in the draw solution, which indicated a breach of membrane integrity (Figure 4A). For instance, at the conclusion of the second scaling-cleaning cycle (Cycle II), Rhodamine WT peak could be clearly identified with concentration of 6 μg L^{-1}, corresponding to an LRV of 4 [41]. More importantly, this 4 LRV credit of the FO membrane was compromised after three gypsum scaling-cleaning cycles.

In order to provide insights into the degree of membrane integrity loss, we also correlated the membrane LRV as a function of pinhole size to quantify the degree of membrane integrity loss during the gypsum scaling (Figure 4B). The SEM images, showing the localization of defects formation near the spacer filaments (Figure 2), cannot accurately reflect membrane integrity loss during the gypsum scaling. Using the calibrated pinhole size-LRV curve (Figure 4B), we demonstrated that membrane integrity loss was equivalent to a membrane with pinhole size of 0.065 μm^2 (Figure 4B) when gypsum scalant accumulated adjacent to spacer filament at the conclusion of three scaling-cleaning cycles.

[Figure 4]

3.3.2 Latex Nanoparticle challenge test

Latex nanoparticle challenge tests offered further insights into the aforementioned FO membrane integrity loss that was equivalent to a pinhole size of 0.065 μm^2 in fluorescent Rhodamine WT challenge test. Dynamic light scattering measurements showed that the particle size distribution in the draw solution became wider and shifted towards the larger particle size range (Figure 5). Specifically, negligible presence of latex particle in the draw solution was observed after first scaling-cleaning cycle, which was evident by the sharp particle size distribution and relative small average particle size of 15 nm (Figure 5B). This result was consistent with the fluorescent Rhodamine WT challenge test where the FO membrane LRV was around 5 with insignificant permeation of Rhodamine WT to the draw solution (Figure 4). However, a significant, progressive increase in the particle size distribution occurred after the second and third scaling-cleaning cycles, with the average particle size rising to 30 and 50 nm. More alarming, particle size distribution in the draw solution exhibited a similar pattern as the feed latex particle after three cleaning-scaling cycles (Figure 5D), indicating the FO membrane integrity was compromised to virus sized particles. This observation agreed well with the results obtained from the fluorescent Rhodamine WT challenge test, both of which suggested that the FO membrane integrity was impaired during gypsum scaling.

[Figure 5]

3.4 Implications

Results reported here have significant implications for both FO membrane module development as well as the deployment of FO membrane in water reuse. In this study, we presented experimental evidence showing FO membrane integrity was compromised during gypsum scaling driven by the preferential accumulation of gypsum scalant adjacent to membrane spacer. Further optimization of FO membrane spacer or novel design of FO module should be considered to minimize the adverse impact on membrane performance. The detection of membrane integrity loss also requires periodic monitoring of FO process in water reuse where the risk of pathogen transport, such as virus, is a concern for impaired FO membrane. In addition, different type or size of tracers should be considered to maximize the relevance of the challenge tests to pathogen rejection when the potential membrane pinhole became larger.

3.5 Conclusion

Results reported here highlighted the FO membrane integrity loss using fluorescent Rhodamin WT tracer and latex nanoparticle, during gypsum scaling with the presence of membrane spacer. Such FO membrane integrity loss was driven by the preferential accumulation of gypsum scalant adjacent to membrane spacer where the needle-shape gypsum potentially compromised FO membrane integrity. More importantly, the routine measurements of FO membrane water and salt (NaCl) permeabilities cannot identify the membrane integrity breach, which warranted the employment of membrane integrity challenge tests by Rhodamine WT tracer and amine-modified latex nanoparticles, respectively. As a result, challenge tests using Rhodamine WT tracer showed that membrane log removal value decreased to 3.5 after three scaling-cleaning cycles, which corresponded to a pinhole size of 0.06 μm^2 on the FO membrane surface. This result was further corroborated by challenge tests using latex nanoparticle where the particle size distribution in the permeate became wider and the average particle size increased over the three scaling-cleaning cycles. Both challenge tests were sensitive enough to identify impaired FO membrane integrity. Results reported here have significant implications for achieving better membrane spacer and module design, as well as demanding periodical monitoring of FO membrane integrity in water reuse.

3.6 Acknowledgements

M.X. thanks the Victoria University for Vice Chancellor Early Career Research Fellowship.

3.7 References

[1] M.A. Shannon, P.W. Bohn, M. Elimelech, J.G. Georgiadis, B.J. Marinas, A.M. Mayes, Science and technology for water purification in the coming decades, Nature, 452 (2008) 301-310.

[2] M. Elimelech, W.A. Phillip, The Future of Seawater Desalination: Energy, Technology, and the Environment, Science, 333 (2011) 712-717.

[3] D.L. Shaffer, J.R. Werber, H. Jaramillo, S. Lin, M. Elimelech, Forward osmosis: Where are we now?, Desalination, 356 (2015) 271-284.

[4] B. Mi, M. Elimelech, Organic fouling of forward osmosis membranes: Fouling reversibility and cleaning without chemical reagents, Journal of Membrane Science, 348 (2010) 337-345.

[5] B. Mi, M. Elimelech, Chemical and physical aspects of organic fouling of forward osmosis membranes, Journal of Membrane Science, 320 (2008) 292-302.

[6] M. Xie, L.D. Nghiem, W.E. Price, M. Elimelech, Impact of organic and colloidal fouling on trace organic contaminant rejection by forward osmosis: Role of initial permeate flux, Desalination, 336 (2014) 146-152.

[7] M. Xie, J. Lee, L.D. Nghiem, M. Elimelech, Role of pressure in organic fouling in forward osmosis and reverse osmosis, Journal of Membrane Science, 493 (2015) 748-754.

[8] G. Chen, Z. Wang, L.D. Nghiem, X.-M. Li, M. Xie, B. Zhao, M. Zhang, J. Song, T. He, Treatment of shale gas drilling flowback fluids (SGDFs) by forward osmosis: Membrane fouling and mitigation, Desalination, 366 (2015) 113-120.

[9] D.L. Shaffer, L.H. Arias Chavez, M. Ben-Sasson, S. Romero-Vargas Castrillón, N.Y. Yip, M. Elimelech, Desalination and Reuse of High-Salinity Shale Gas Produced Water: Drivers, Technologies, and Future Directions, Environmental Science & Technology, 47 (2013) 9569-9583.

[10] B.D. Coday, P. Xu, E.G. Beaudry, J. Herron, K. Lampi, N.T. Hancock, T.Y. Cath, The sweet spot of forward osmosis: Treatment of produced water, drilling wastewater, and other complex and difficult liquid streams, Desalination, 333 (2014) 23-35.

[11] B.D. Coday, N. Almaraz, T.Y. Cath, Forward osmosis desalination of oil and gas wastewater: Impacts of membrane selection and operating conditions on process performance, Journal of Membrane Science, 488 (2015) 40-55.

[12] A. Achilli, T.Y. Cath, E.A. Marchand, A.E. Childress, The forward osmosis membrane bioreactor: A low fouling alternative to MBR processes, Desalination, 239 (2009) 10-21.

[13] R.W. Holloway, J. Regnery, L.D. Nghiem, T.Y. Cath, Removal of Trace Organic Chemicals and Performance of a Novel Hybrid Ultrafiltration-Osmotic Membrane Bioreactor, Environmental Science & Technology, 48 (2014) 10859-10868.

[14] J. Zhang, W.L.C. Loong, S. Chou, C. Tang, R. Wang, A.G. Fane, Membrane biofouling and scaling in forward osmosis membrane bioreactor, Journal of Membrane Science, 403–404 (2012) 8-14.

[15] L. Chen, Y. Gu, C. Cao, J. Zhang, J.-W. Ng, C. Tang, Performance of a submerged anaerobic membrane bioreactor with forward osmosis membrane for low-strength wastewater treatment, Water Research, 50 (2014) 114-123.

[16] M. Xie, L.D. Nghiem, W.E. Price, M. Elimelech, A Forward Osmosis–Membrane Distillation Hybrid Process for Direct Sewer Mining: System Performance and Limitations, Environmental Science & Technology, 47 (2013) 13486-13493.

[17] M.S. Diallo, G. Baier, B.A. Moyer, B. Hamelers, Critical Materials Recovery from Solutions and Wastes: Retrospective and Outlook, Environmental Science & Technology, 49 (2015) 9387-9389.

[18] J. Zhang, Q. She, V.W.C. Chang, C.Y. Tang, R.D. Webster, Mining Nutrients (N, K, P) from Urban Source-Separated Urine by Forward Osmosis Dewatering, Environmental Science & Technology, 48 (2014) 3386-3394.

[19] M. Xie, L.D. Nghiem, W.E. Price, M. Elimelech, Toward Resource Recovery from Wastewater: Extraction of Phosphorus from Digested Sludge Using a Hybrid Forward Osmosis–Membrane Distillation Process, Environmental Science & Technology Letters, 1 (2014) 191-195.

[20] B.D. Coday, C. Hoppe-Jones, D. Wandera, J. Shethji, J. Herron, K. Lampi, S.A. Snyder, T.Y. Cath, Evaluation of the transport Parameters and physiochemical properties of forward osmosis Membranes after treatment of produced water, Journal of Membrane Science.

[21] Y.-N. Wang, E. Järvelä, J. Wei, M. Zhang, H. Kyllönen, R. Wang, C.Y. Tang, Gypsum scaling and membrane integrity of osmotically driven membranes: The effect of membrane materials and operating conditions, Desalination, 377 (2016) 1-10.

[22] S. Singh, R.K. Henderson, A. Baker, R.M. Stuetz, S.J. Khan, Characterisation of reverse osmosis permeates from municipal recycled water systems using fluorescence spectroscopy: Implications for integrity monitoring, Journal of Membrane Science, 421–422 (2012) 180-189.

[23] M.-L. Pype, D. Patureau, N. Wery, Y. Poussade, W. Gernjak, Monitoring reverse osmosis performance: Conductivity versus fluorescence excitation–emission matrix (EEM), Journal of Membrane Science, 428 (2013) 205-211.

[24] M. Kumar, S. Adham, J. DeCarolis, Reverse osmosis integrity monitoring, Desalination, 214 (2007) 138-149.

[25] B. Mi, C.L. Eaton, J.-H. Kim, C.K. Colvin, J.C. Lozier, B.J. Mariñas, Removal of biological and non-biological viral surrogates by spiral-wound reverse osmosis membrane elements with intact and compromised integrity, Water Research, 38 (2004) 3821-3832.

[26] B. Mi, D.G. Cahill, B.J. Mariñas, Physico-chemical integrity of nanofiltration/reverse osmosis membranes during characterization by Rutherford backscattering spectrometry, Journal of Membrane Science, 291 (2007) 77-85.

[27] X. Huang, J.H. Min, W. Lu, K. Jaktar, C. Yu, S.C. Jiang, Evaluation of methods for reverse osmosis membrane integrity monitoring for wastewater reuse, Journal of Water Process Engineering, 7 (2015) 161-168.

[28] T.Y. Cath, M. Elimelech, J.R. McCutcheon, R.L. McGinnis, A. Achilli, D. Anastasio, A.R. Brady, A.E. Childress, I.V. Farr, N.T. Hancock, J. Lampi, L.D. Nghiem, M. Xie, N.Y. Yip,

Standard Methodology for Evaluating Membrane Performance in Osmotically Driven Membrane Processes, Desalination, 312 (2013) 31-38.

[29] A. Tiraferri, N.Y. Yip, A.P. Straub, S. Romero-Vargas Castrillon, M. Elimelech, A method for the simultaneous determination of transport and structural parameters of forward osmosis membranes, Journal of Membrane Science, 444 (2013) 523-538.

[30] M. Park, J.H. Kim, Numerical analysis of spacer impacts on forward osmosis membrane process using concentration polarization index, Journal of Membrane Science, 427 (2013) 10-20.

[31] R. Valladares Linares, S.S. Bucs, Z. Li, M. AbuGhdeeb, G. Amy, J.S. Vrouwenvelder, Impact of spacer thickness on biofouling in forward osmosis, Water Research, 57 (2014) 223-233.

[32] H. Zhang, S. Cheng, F. Yang, Use of a spacer to mitigate concentration polarization during forward osmosis process, Desalination, 347 (2014) 112-119.

[33] Y. Wang, F. Wicaksana, C.Y. Tang, A.G. Fane, Direct Microscopic Observation of Forward Osmosis Membrane Fouling, Environmental Science & Technology, 44 (2010) 7102-7109.

[34] S. Zou, Y.-N. Wang, F. Wicaksana, T. Aung, P.C.Y. Wong, A.G. Fane, C.Y. Tang, Direct microscopic observation of forward osmosis membrane fouling by microalgae: Critical flux and the role of operational conditions, Journal of Membrane Science, 436 (2013) 174-185.

[35] G. An, J. Lin, J. Li, X. Li, X. Jian, Non-invasive measurement of membrane scaling and cleaning in spiral-wound reverse osmosis modules by ultrasonic time-domain reflectometry with sound intensity calculation, Desalination, 283 (2011) 3-9.

[36] G.Y. Chai, A.R. Greenberg, W.B. Krantz, Ultrasound, gravimetric, and SEM studies of inorganic fouling in spiral-wound membrane modules, Desalination, 208 (2007) 277-293.

[37] A.I. Radu, L. Bergwerff, M.C.M. van Loosdrecht, C. Picioreanu, A two-dimensional mechanistic model for scaling in spiral wound membrane systems, Chemical Engineering Journal, 241 (2014) 77-91.

[38] M. Xie, L.D. Nghiem, W.E. Price, M. Elimelech, Impact of humic acid fouling on membrane performance and transport of pharmaceutically active compounds in forward osmosis, Water Research, 47 (2013) 4567-4575.

[39] M. Xie, M. Zheng, P. Cooper, W.E. Price, L.D. Nghiem, M. Elimelech, Osmotic dilution for sustainable greenwall irrigation by liquid fertilizer: Performance and implications, Journal of Membrane Science, 494 (2015) 32-38.

[40] S. Surawanvijit, J. Thompson, A. Rahardianto, V. Frenkel, Y. Cohen, Pulsed marker method for real-time detection of reverse osmosis membrane integrity loss, Desalination, 370 (2015) 25-32.

[41] L.F. Greenlee, D.F. Lawler, B.D. Freeman, B. Marrot, P. Moulin, Reverse osmosis desalination: Water sources, technology, and today's challenges, Water Research, 43 (2009) 2317-2348.

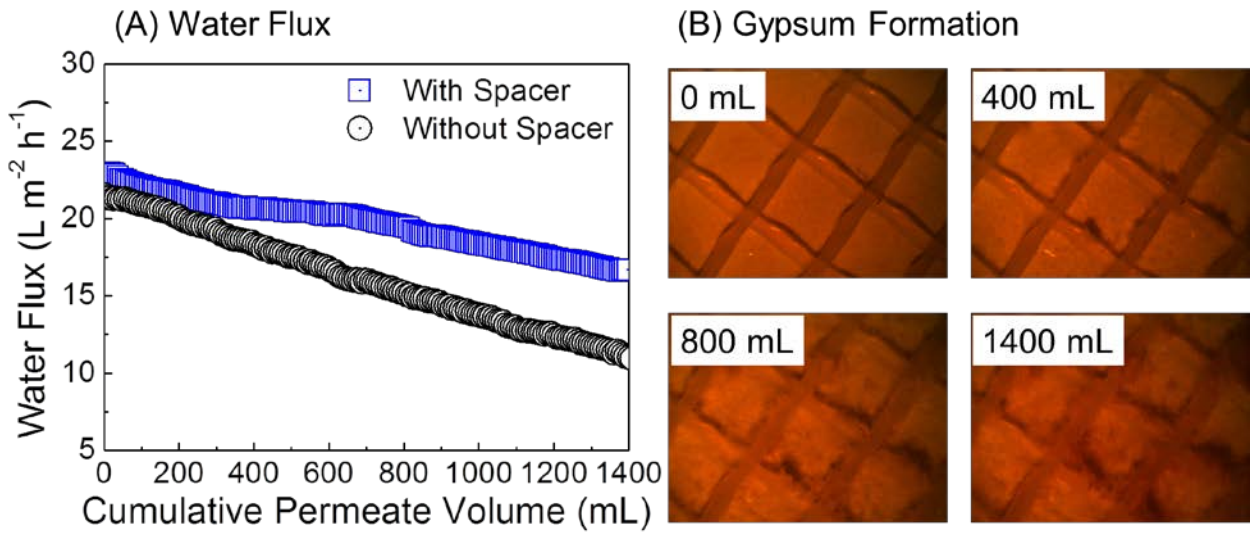

Figure 1: Gypsum scaling during forward osmosis filtration: (A) water flux decline as a function of cumulative permeate volume with and without membrane spacer; and (B) real-time microscopic observation at specific cumulative permeate volumes for experiments with spacer. Experimental conditions were: the scaling solution contains 35 mM $CaCl_2$, 20mM Na_2SO_4, and 19 mM NaCl, with a gypsum saturation index of 1.3. A 2 M NaCl draw solution was used in FO. Diamond-patterned, polypropylene spacers (65 mil (1.651 mm)) were used in feed and draw solution sides, crossflow velocity of 9 cm/s, ambient pH (pH 6.8), and temperature of 25.0 ± 0.1°C. Representative real-time images were taken at specific cumulative permeate volumes. Note that the flux for the fouled membrane is corrected by the initial flux in the fouling experiments.

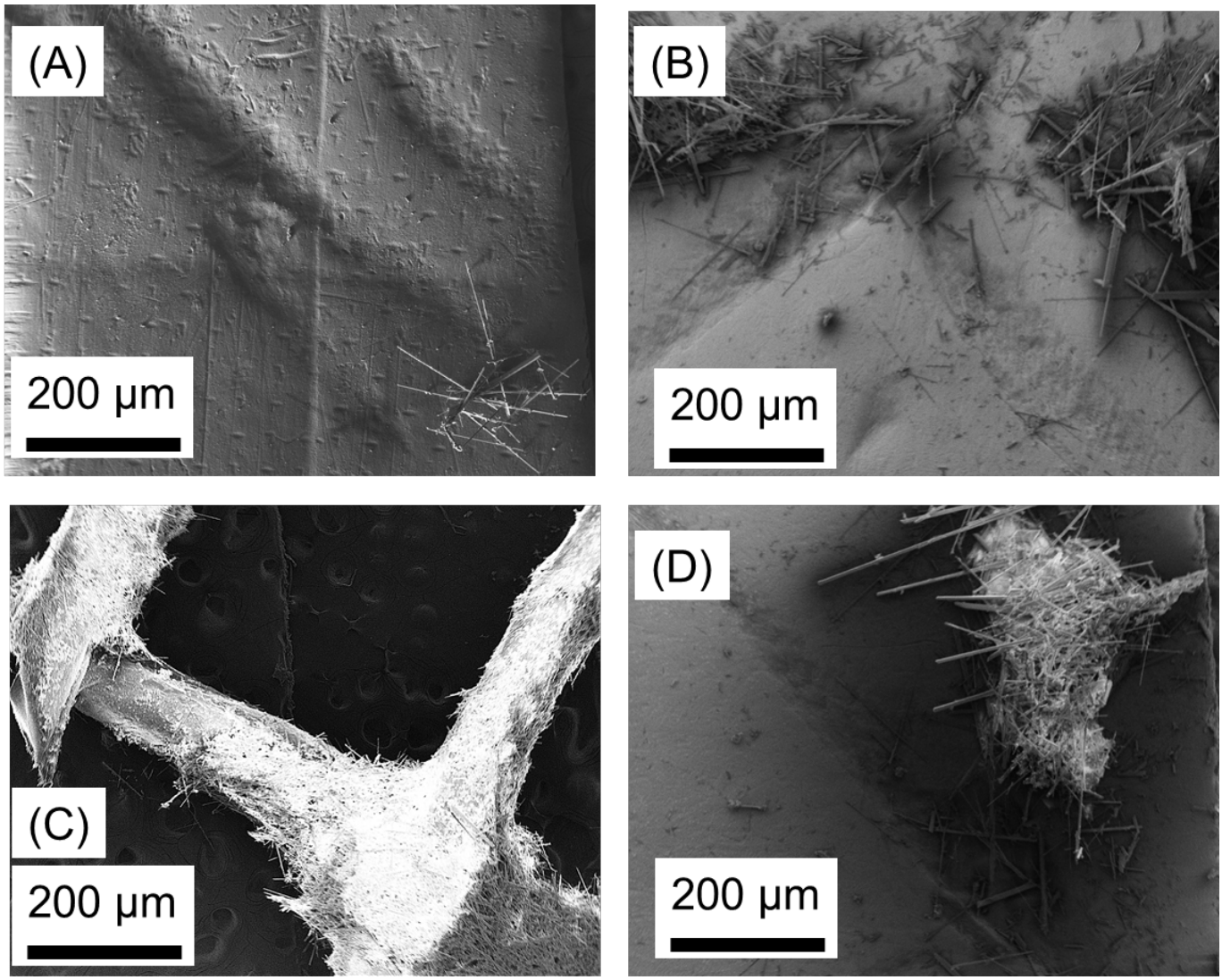

Figure 2: SEM micrographs of (A) FO membrane and (C) spacer at the conclusion of gypsum scaling experiments. The potential impaired membrane was revealed in (B) and (D) where a clear indent of spacer was observed.

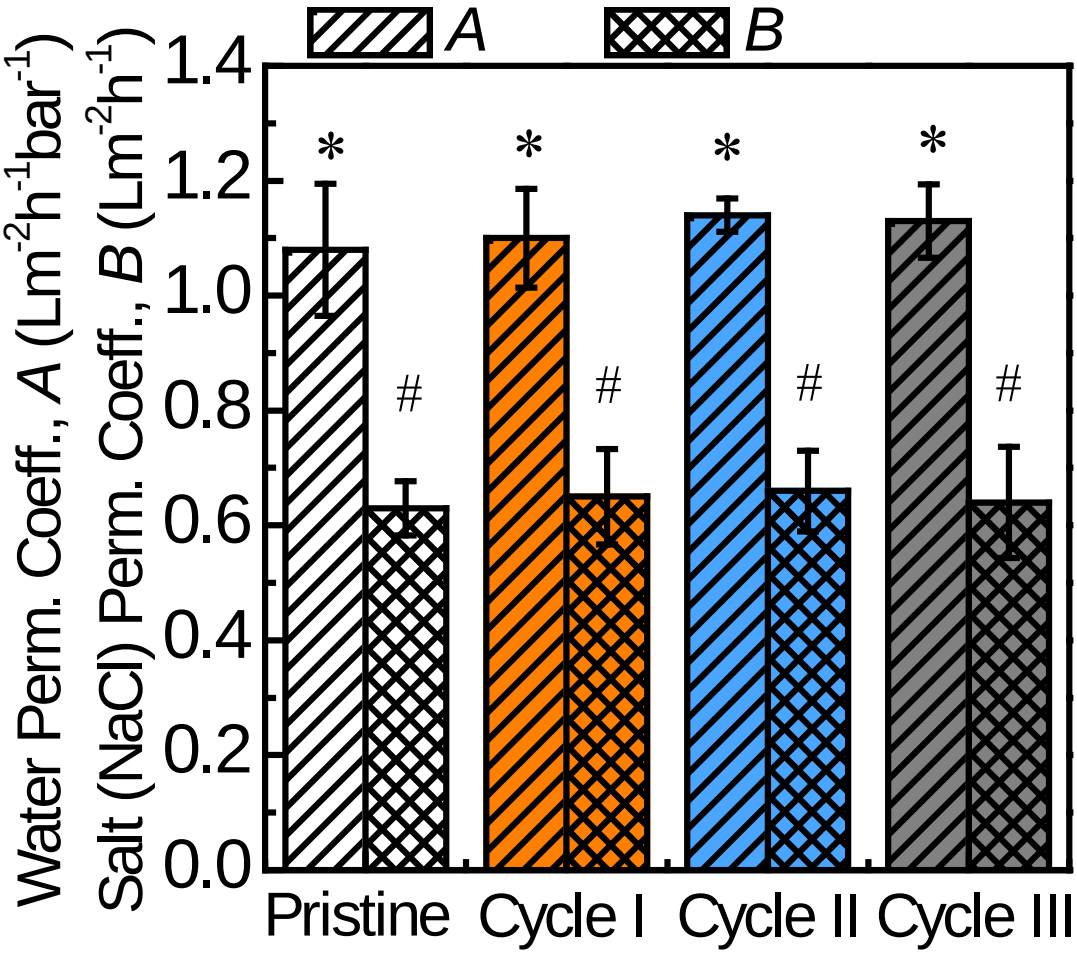

Figure 3: Water and salt (NaCl) permeabilities of pristine membrane and membrane at the conclusion of each scaling-cleaning cycle. These two key membrane transport parameters were measured *in situ* using a four-step method in a single FO experiment. The NaCl draw solution concentration in each step was 0.2, 0.4, 0.7, and 1.2 M. Asterisk and hash symbols above the bar indicates measurement differences were statistically insignificant (student *t*-test, *p* value>0.05).

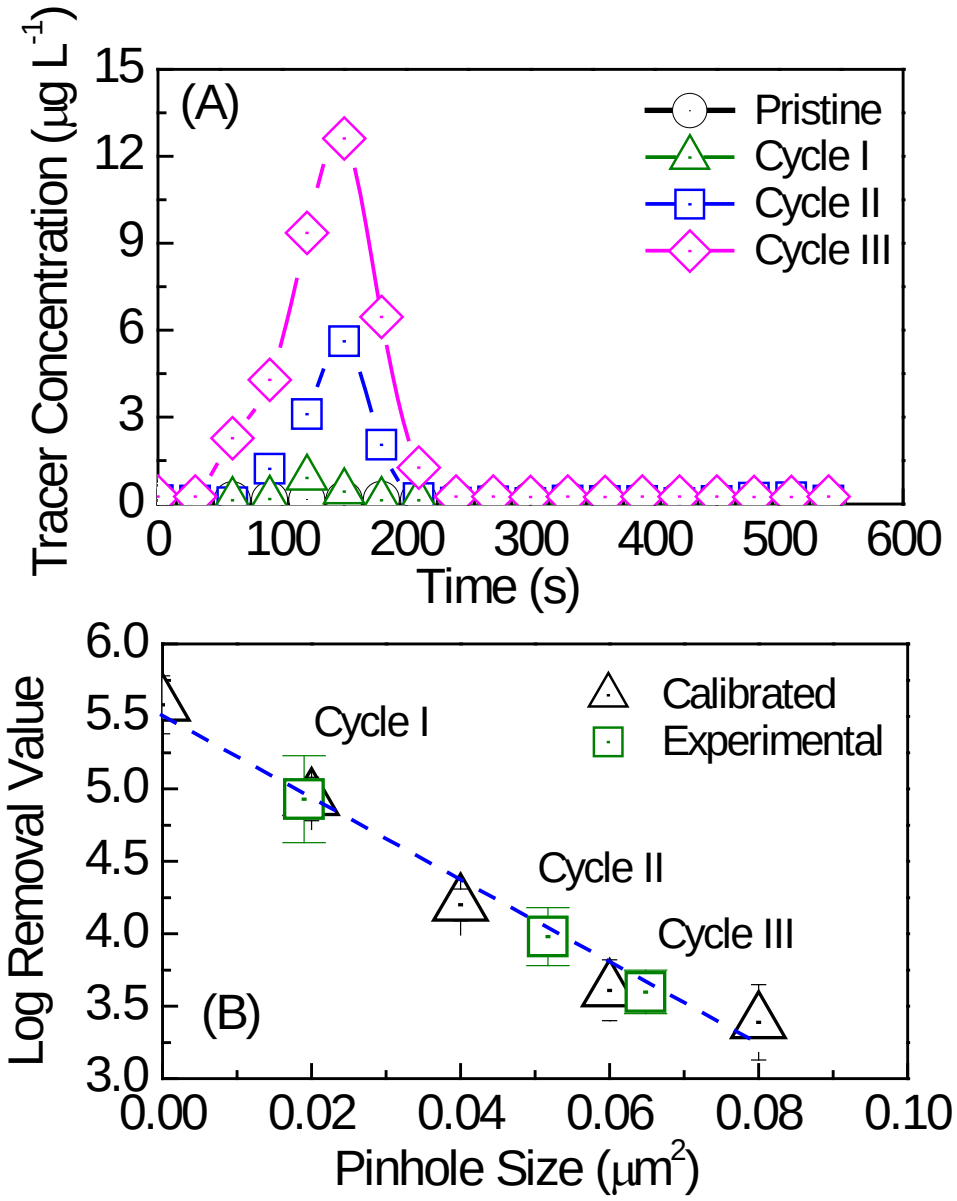

404

405 **Figure 4:** Membrane integrity challenge test using fluorescent Rhodamine WT tracer. (A)
406 Rhodamine WT concentration in the draw solution as a function of time (B) correlation Log
407 Removal Value (LRV) with membrane pinhole size. Black triangular symbols represent
408 membrane LRV obtained from artificial membrane pinhole; the green square symbols were LRV
409 of membrane at the conclusion of each scaling-cleaning cycle; the blue dotted line was drawn to
410 guide the eye. Experimental conditions were: the FO membrane cell was operated in one-pass
411 mode where fluorescent Rhodamine WT solution of 50 mg/L was injected into the FO feeding
412 tube for 60 seconds at a crossflow rate of 1 L/min. At the same time, the draw solution at the
413 crossflow rate of 1 L/min was sampled every 10 seconds for a total of 540 seconds.

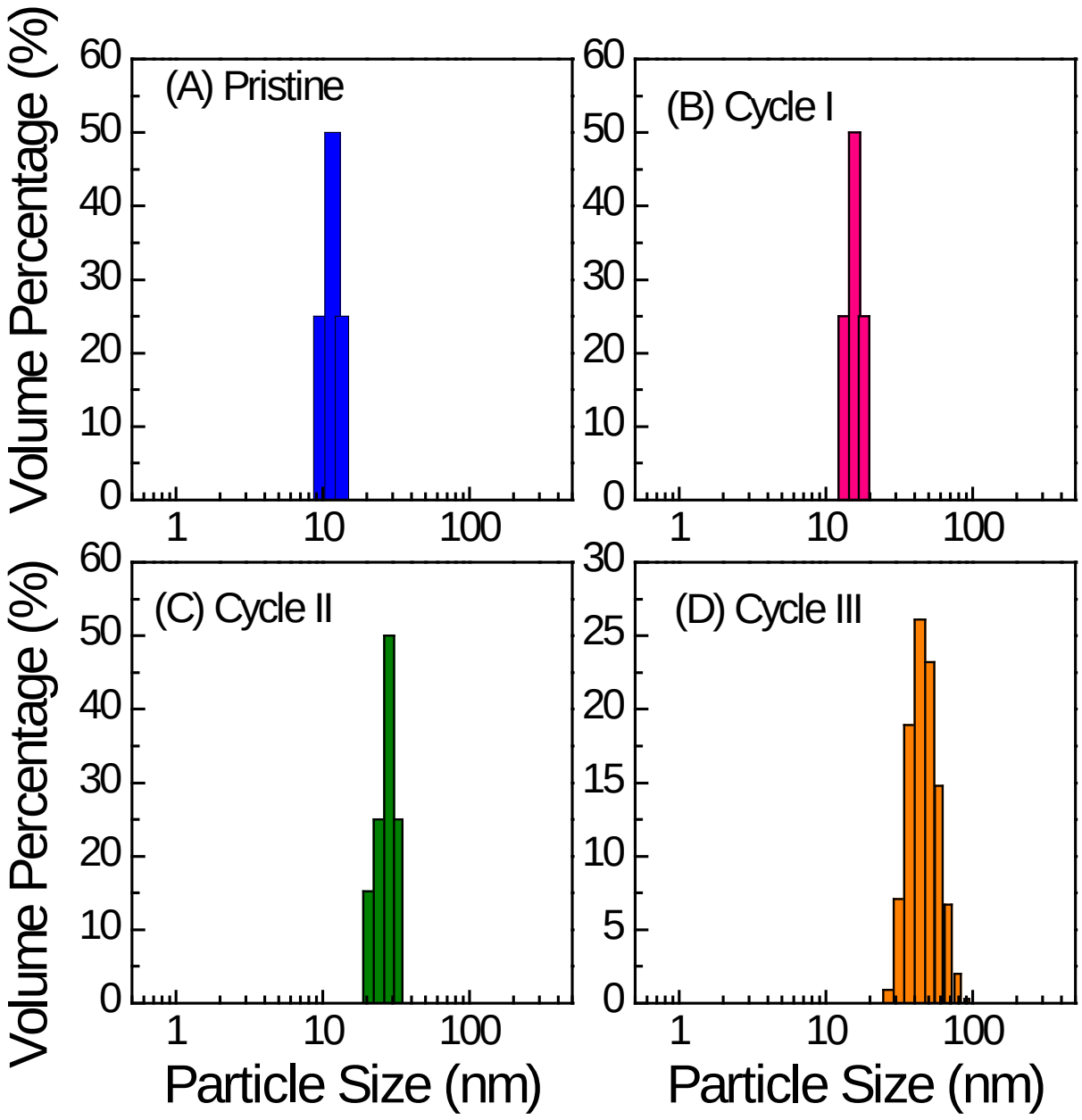

Figure 5: Membrane integrity challenge test using amine-modified latex nanoparticles. Particle size distribution of draw solution using (A) pristine membrane, and (B)-(D) membrane at the conclusion of each scaling-cleaning cycle. The particle size distribution was determined by dynamic light scattering. Experimental conditions were: the FO membrane cell was operated in single-pass mode where amine-modified latex nanoparticle solution of 20 mg/L was injected into the FO feeding tube for 60 seconds at a crossflow rate of 1 L/min. At the same time, the draw solution at a crossflow rate of 1 L/min was sampled for a total of 540 seconds.